Delft University of Technology

bachelor thesis

Study of DNA origami plates on graphene nanopores

Author:
Thierry van Thiel

Supervisors:
Stephanie Heerema
Adithya Ananth
Prof.dr. Cees Dekker

May 2015

Abstract

Combining DNA origami with solid-state nanopores has been gaining an increasing amount of attention due to its potential for biosensing applications. Accordingly, origami plate dockings onto conventional solid-state silicon nitride pores with membranes of 20nm thick were previously studied. Here, we examine whether graphene, with its single layer of carbon atoms, poses advantages over silicon-nitride pores. The conductance blockades due to origami plate dockings were characterized as a function of salt concentration and applied bias voltage and compared to the silicon-nitride data. As expected, it was found that conductance blockades increase with salt concentration and voltage. The relative conductance drop in graphene was however found to be similar to that for silicon nitride pores, whereas theory predicts that the blockade signal is larger in graphene pores. We have further compared the root-mean-squared noise levels of the ionic current through hybrid graphene-origami pores and bare pores, and found that the noise in the hybrid pores was slightly higher than in the bare pore current. Finally, it was tested whether the plates stick to the graphene pore in presence of EDTA. This was done by docking the plates and subjecting them to a negative ramping voltage. Without EDTA, no evidence of sticking was found, whereas with EDTA, 88.2% of docked plates appeared to be sticking.

Acknowledgements

Writing this thesis has been a long process and I could not have done it without help. First of all, I would like to thank prof.dr.Cees Dekker for allowing me to take part in this project and for his advice during group meetings. I would also like to thank my daily supervisors, Stephanie and Adi, for teaching me how to perform the experiments, for their advice and their feedback on my writing. I want to thank my sister Eva, for aiding me in fabricating some artistic drawings of nanopores and Karlijn for her moral support, helping me conduct theories and proofreading. Lastly, I want to thank the entire nanopore group for giving me the opportunity to work in a stimulating, professional and mostly pleasant environment. I have learned much about conducting scientific experiments, interpreting measurements and reporting on the results. I am very grateful and will take this new found knowledge with to future projects.

Contents

1 Introduction **7**

2 Theory **9**
2.1 DNA . . . 9
2.1.1 Primary structure of DNA . . . 9
2.1.2 Secondary structure of DNA . . . 10
2.1.3 Holliday-junction . . . 10
2.2 DNA origami . . . 12
2.2.1 Folding DNA into two-dimensional shapes . . . 12
2.2.2 Three-dimensional structures . . . 13
2.3 Graphene . . . 14
2.3.1 Structure and dimensions . . . 14
2.3.2 Properties . . . 15
2.4 Conductance of nanopore hybrids . . . 15
2.4.1 Bare pore conductance . . . 15
2.4.2 Relative conductance . . . 17
2.4.3 Noise in graphene nanopores . . . 18

3 Methods **20**
3.1 Nanopore fabrication . . . 20
3.1.1 Wedging transfer . . . 20
3.1.2 TEM drilling . . . 21
3.2 Nanoplate docking . . . 23
3.3 Sticking of plates to the pore . . . 24

4 Results and Discussion **25**
4.1 Characterization of the relative conductance . . . 25
4.2 Sticking of plates to graphene nanopores . . . 31
4.3 Noise of hybrid and bare pores . . . 34

5 Conclusions **36**

6 Outlook **38**

Appendices **39**

A Data tables and buckling voltage distribution **40**

List of Figures

2.1 Secondary structure of a two-base dsDNA molecule 11
2.2 Diagram of the DNA double helix 11
2.3 Both configurations of the Holliday-junction 11
2.4 Illustrative drawing of a DNA origami structure 12
2.5 Honeycomb pleat-based strategy 13
2.6 Schematic display of the structure of graphene 14
2.7 Schematic drawing of a DNA strand translocating through a nanopore 16
2.8 Cross section of a thick and thin nanopore membrane 17

3.1 Graphene flakes on a Si/SiO2 wafer 22
3.2 Graphene flakes embedded in a CAB patch 22
3.3 STEM image of a graphene nanopore 22
3.4 Experimental setup 24

4.1 Distribution of the relative conductance drop in 1.0M KCl 26
4.2 Distribution of the relative conductance drop in 0.6M KCl 27
4.3 Distribution of the relative conductance drop in 0.3M KCl 28
4.4 Plate permeability and relative conductance of graphene and SiN . . 29
4.5 Comparison between I-V curves of hybrids and a bare pore 31
4.6 Negative I-V curves of hybrid pores with EDTA 32
4.7 Negative I-V curves of hybrid pores without EDTA 32
4.8 Negative I-V curves of hybrids showing plate captures (no EDTA) . . 33
4.9 Noise of graphene hybrids and bare pores 35

A.1 Mechanical buckling voltage distribution 42

List of Tables

A.1 Relative conductance 41
A.2 Plate permeability 41
A.3 Normalized noise values before docking 41
A.4 Normalized noise values after docking 41
A.5 Mechanical buckling voltage 42

Chapter 1

Introduction

Physicists have tried to tackle the many questions of biology for a long time, this discipline is known as biophysics. While biologists and biochemists try to gain insight in biological processes by performing bulk experiments, physicists use and develop technology for studying biology at the scale of a single molecule. One of these technologies is the *nanopore*. Early nanopores were made by inserting an α-haemolysin protein secreted by the *Staphylococcus aureus* bacteria into a lipid bilayer membrane, creating a so-called biological nanopore with a channel diameter of 1.4nm[1]. Years later, the field of solid-state nanopores emerged, offering a number of advantages over biological pores such as better stability and more control over pore geometry[2]. Another advantage is the possibility to combine nanopores and other nanotechnology such as DNA origami, a technique for folding DNA nanostructures. This opens up many new possibilities for DNA and protein sensing. Solid-state nanopores were created by drilling a hole into an insulating medium such as SiN. Pores were several nanometers in diameter and had channels of tens of nanometers long. As DNA sequencing is one of the prime objectives of nanopore research, the pore channels were much too long to achieve single base-pair resolution. This is where graphene, a one atom thick layer of carbon, came into play.

Combining DNA origami with solid-state nanopores introduces a great many possibilites for changing and enhancing pore properties and features. One could for instance, think of a plate design with a loose DNA strand on top, or spanned across a central aperture for protein sensing purposes. Since DNA repels DNA, a plate with a central aperture could also be used in DNA translocation experiments to prevent translocating strands from clogging the pore. This could be especially useful in graphene nanopores, since ssDNA is prone to stick to graphene[3,4].

Our group previously investigated the behaviour of DNA origami on SiN nanopores[5]. In this thesis, the effect of DNA nanoplates docked onto graphene nanopores on pore conductance and signal-to-noise ratio shall be investigated as a function of salt and applied bias voltage. The results shall be compared to SiN. We also hypothesise, that dsDNA nanoplates stick to graphene in the presence of EDTA (ethylenediaminetetraacetic acid). Sticking would enable better fixation of the plates to the pore and would thus result in a more stable hybrid. This could prove very useful in experiments and constitutes a possible advantage graphene poses over traditional SiN membranes. In the next chapter, the theory regarding DNA origami and graphene

nanopores shall be discussed and in Chapter 3 the experimental methods shall be reviewed. In Chapter 4 the results of the plate docking and sticking experiments shall be presented and discussed. In Chapter 5 conclusions shall be drawn and in Chapter 6 possible future research shall be looked at. This research is conducted at the Bionanoscience department of the Faculty of Applied Sciences, Delft University of Technology.

Chapter 2

Theory

2.1 DNA

DNA or deoxyribonucleic acid is the molecule that carries the genetic information for life. It is a long polymer chain molecule that is stored in the cells and contains a code which can be transcripted to RNA and subsequently translated to amino acids. These amino acids polymerize to form proteins, which serve numerous purposes within a living cell.

While the biological functions and properties of DNA are a very interesting topic, they are outside of the scope of this thesis. We are interested in applying folded DNA structures to graphene nanopores. Because of the specificity of Watson-Crick base-pairing, which shall be discussed later, DNA is an excellent material for 'bottom-up fabrication'. Bottom-up fabrication utilizes the intrinsic properties of molecules and individual atoms to self-assemble into nanostructures. The folding of DNA strands into a desired shape, known as *DNA origami*, is an example of such assembly. In order to understand how DNA origami works we shall first discuss the structure of DNA and Holliday junctions briefly.

2.1.1 Primary structure of DNA

Deoxyribonucleic acid is a molecule that consists of three segments, a sugar, a phosphate group and a nucleic base. The sugar is 2-D-deoxyribose ($C_5H_{10}O_4$), a derivate of ribose ($C_5H_{10}O_5$) through loss of an oxygen atom at the 2' end. These sugars polymerize into a chain via phosphodiester bonds at the 3' and 5' carbons. This constitutes a phosphate-deoxyribose polymer which is referred to as the 'backbone' of a DNA strand. To the 1' carbon of each monomer a nitrogen-containing base is attached. There are four nucleic bases in total, A(denine), G(uanine), C(ytosine) and T(hymine). The bases attached to the backbone form a single DNA strand, we shall refer to this as ssDNA (single-stranded DNA). The structure of the four bases lend themselves to form hydrogen bonds with one another. Adenine can form two hydrogen bonds with thymine and guanine can form three with cytosine. This means that two strands of ssDNA can bond together to form double-stranded DNA. Adenine always pairs with thymine (AT) and guanine always pairs with cytosine

(GC). This is known as Watson-Crick base-pairing[6]. See figure 2.1 on page 11, the dashed lines represent the hydrogen bonds responsible for the base-pairing. The AG strand is oriented exactly opposite to the complementary CT strand. The left strand is said to run from the 5' end to the 3' end and the right strand from the 3' end to the 5' end, therefore they each have their free phosphate group at opposite ends. Subsequently a dsDNA molecule is polar and highly negatively charged[7].

2.1.2 Secondary structure of DNA

There are multiple interactions between the two strands, both hydrophobic and hydrophilic. As discussed in the previous section, bases form hydrogen bonds with one another. But purine and pyrimidine also contain hydrophobic aromatic rings. These rings have hydrophobic interactions perpendicular to the direction of the hydrogen bonds. As the hydrogen bonds are formed at an angle, it causes the two strands to coil around each other to form a double helix. This helical structure was proposed by Watson and Crick in 1953[6]. The type described by Watson and Crick would later be known as B-DNA[8]. Its helix has roughly ten nucleotides (3.4nm in length) per turn and is right-handed. See figure 2.2. The part where the backbones are close together is referred to as the minor groove, whereas the part where they are further apart is called the major groove.

2.1.3 Holliday-junction

The Holliday junction, named after Robert Holliday is a heteroduplex DNA structure that was used to explain certain gene-conversion phenomena during meiosis in fungi[9]. It consists of two strands of dsDNA crossing over into each other. There are two possible configurations. Both outer strands of ssDNA can run parallel to each other, or antiparallel where one strand runs from the 3' to the 5' end and the other oppositely. In parallel the inner strands crossover whereas in the antiparallel orientation, they do not. The parallel orientation corresponds to an open-planar configuration and the anti-parallel to a stacked X-configuration. Electrostatic repulsion by e.g. metal-ions has influence on which configuration is preferable. In the presence of metal ions the stacked X-configuration is more likely[9]. Figure 2.3 displays the open planar-configuration (left) and the stacked X-configuration (right)[10].

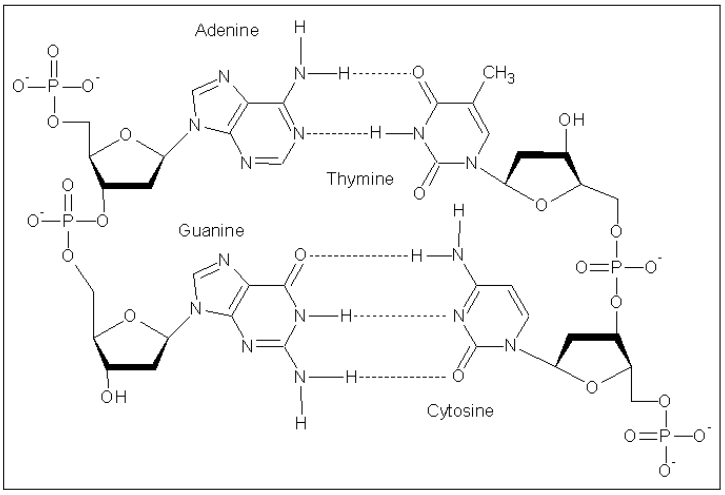

Figure 2.1: Primary structure of a two-base dsDNA molecule

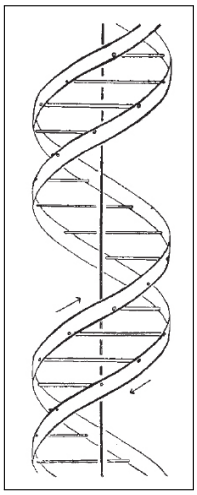

Figure 2.2: Diagram of the DNA double helix[6]

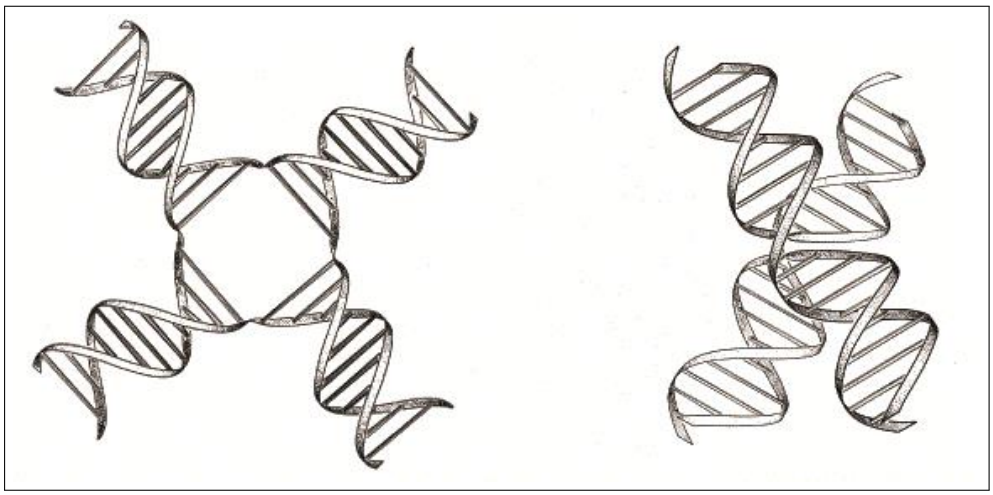

Figure 2.3: Both configurations of the Holliday-junction[10]

2.2 DNA origami

DNA origami was first introduced in 2006 by Paul Rothemund[11]. He devised a number of steps to create a bottom-up nanostructure from nucleic acids. The technique is a relatively simple way to create a wide variety of different nanostructures. In the following paragraphs it will be described how individual DNA strands can fold into a chosen shape.

2.2.1 Folding DNA into two-dimensional shapes

First a geometric model is made which roughly resembles the desired shape. This model consists of 'building blocks' of ssDNA comprising 10.67 base pairs or roughly one helical turn. All of these blocks together form a raster, linked by vertical crossover points that are incorporated every 1.5 turns. A strand of ssDNA is chosen to run through the raster. This is referred to as the scaffold strand. It twists at the end of each row and then follows the adjacent one. A number of oligonucleotide 'staple strands' are used to complement the scaffold strand and create additional crossovers. To reduce strain, crossover strands are chosen with alternating groove pattern in alternating columns.

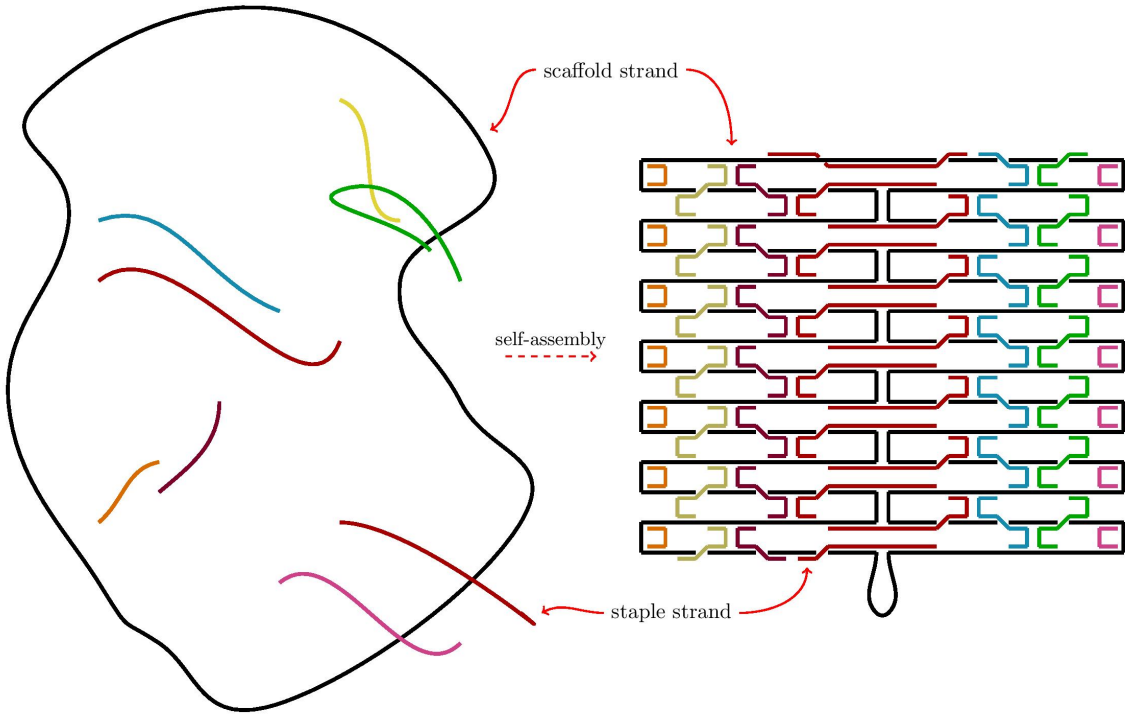

Figure 2.4: Illustrative drawing of the folding of a DNA origami nanostructure

See figure 2.4. The black line represents the scaffold and the coloured lines represent the staple strands. Staple strands intertwine with multiple rows of scaffold through heteroduplex Holliday-junctions. No base on the scaffold is left unpaired. It is critical that the staple strands bind only to their designated binding spot and not to each other or any other spot on the scaffold. Therefore their sequence has to be

determined carefully. Software for designing DNA origami structures is available, an example is caDNAno[12] . A purified solution of staple strands is mixed with the scaffold strand. In this mixture, it is made sure that there is a surplus of staple strands. The mixture is heated to 65° Celsius rapidly and then cooled to room temperature over a timespan of two hours[5]. During this process the strands self-assemble into the designed structure.

2.2.2 Three-dimensional structures

The method discussed before is used to design two-dimensional structures. It can however, be adapted to fold three-dimensional shapes as well. Douglas et al. describe a way they call the honeycomb pleat-based strategy[13] . Here the adjacent rows are not connected using staple strands, but using phosphate linkages. The staple strands rather, are used to link helices two rows over, causing the initially flat structure to fold into a three dimensional shape of three layers. This method is not limited to flat layers. A honeycomb shape is created by giving helix *m+1* a preferred attachment angle to helix *m* of 120° relative to helix *m-1*. This angle is determined by the relative shift between the Holliday-junctions of helix *m+1* to *m* versus helix *m-1* to *m*. See figure 2.5 for a detailed illustration[13].

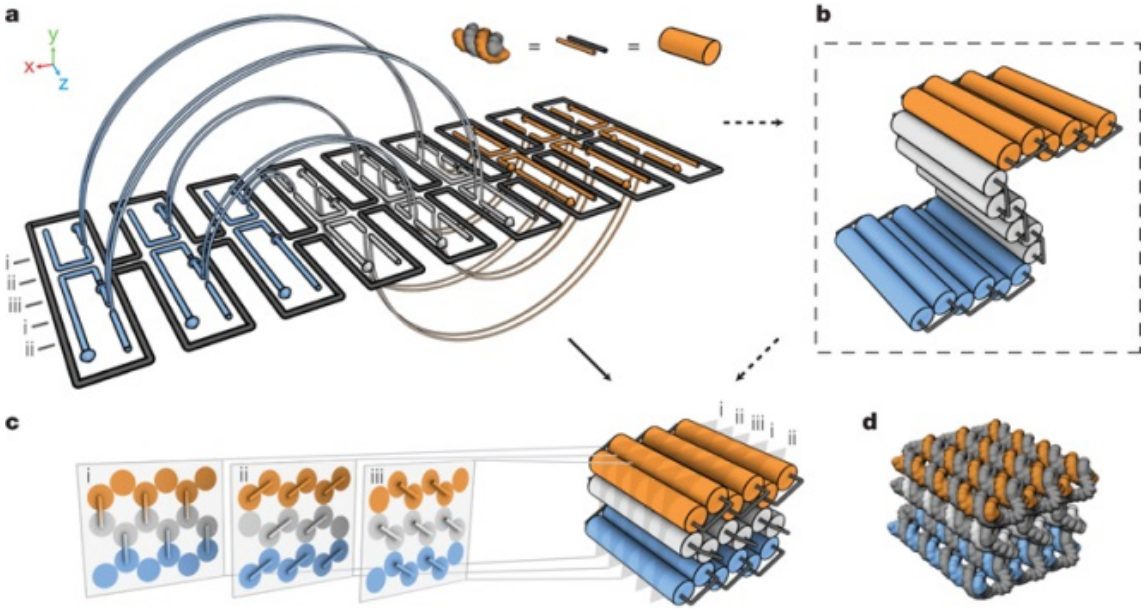

Figure 2.5: ***a*****: Double helices comprised of scaffold (grey) and staple strands (orange, white, blue) run parallel to the z-axis to form an unrolled two-dimensional schematic of the target shape. Phosphate linkages form crossovers between adjacent helices, with staple crossovers bridging different layers shown as semicircular arcs.** ***b*****: Cylinder model of a half-rolled conceptual intermediate. Cylinders represent double helices, with loops of unpaired scaffold strand linking the ends of adjacent helices.** ***c*****: Cylinder model of folded target shape. The honeycomb arrangement of parallel helices is shown in cross-sectional slices (i–iii) parallel to the x–y plane, spaced apart at seven base-pair intervals that repeat every 21 base pairs. All potential staple crossovers are shown for each cross-section.** ***d*****: Atomistic DNA model of shape from c[13]**

2.3 Graphene

Graphene is the term for a two-dimensional lattice of carbon atoms. In other words it is a carbon layer of only one atom thick. Because two-dimensional materials were believed to be thermodynamically unstable, free-standing graphene was thought not to exist. This hypothesis however, was proven wrong in 2004[14]. Novoselov et al. were able to find flakes of graphene monolayers, by means of mechanical exfoliation on an oxidised Si-wafer. In this chapter its atomic structure, dimensions and material properties shall be discussed.

2.3.1 Structure and dimensions

Graphite consists of layers of graphene coupled by weak van der Waals-forces in an ABAB fashion[15]. This results in a hexagonally symmetrical lattice in the horizontal plane. Monolayer graphene is just a single layer of graphite.

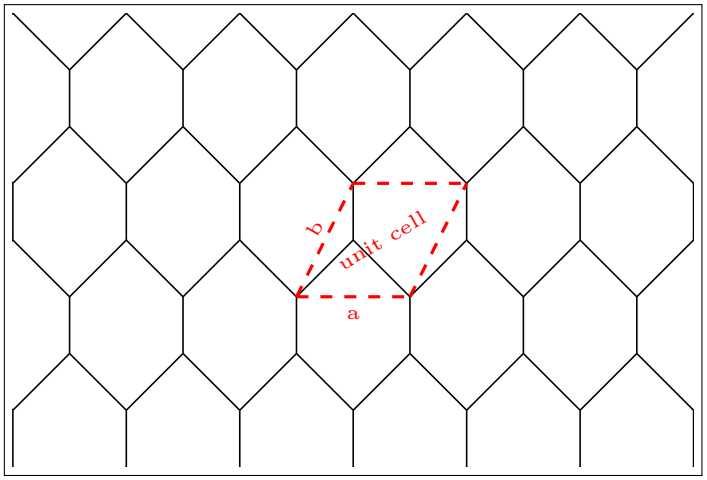

Figure 2.6: Schematic display of the structure of graphene

See figure 2.6. The vectors **a** and **b** in 2.6 are the lattice vectors given by $\vec{a} = (1\ 0)$ and $\vec{b} = (1/2\ \sqrt{3})$. Each carbon atom is bound to another via one σ- and one π-bond. The valence of carbon is four, this means there is one free π-electron and two free electrons per unit-cell. This creates a cloud of electrons on both sides of the sheet. Ishigama et al. managed to get a subnanometer resolved image using Scanning Tunneling Microscopy (STM)[16]. They found that the unit cells are spaced roughly 2.5 Å apart. They also report the thickness of a graphene layer deposited on a SiO_2 substrate to be 4.2 Å in vacuum at the edges, compared to a theoretical prediction of 3.4 Å. In air however, a thickness of 9 Å was measured. This discrepancy was concluded to be due to ambient species (nitrogen, oxygen, argon or water) between the substrate and the graphene. Whereas it is almost infinitely thin, the lateral dimensions of graphene can be in the order of microns[17], this is one of the features that makes it an excellent material for nanotechnology.

2.3.2 Properties

Graphite is a semimetal, whereas graphene is a gapless semi-conductor[18]. The free π-electrons in a graphene lattice have zero effective mass. A consequence of this is that electrons can cover sub-micrometer distances without scattering[19]. The conductivity of graphene is quite poor, but this can be enhanced greatly by using doping. Applications of doped graphene's excellent conductivity include quantum dots, p-n junctions, nanoribbons, quantum point contacts and fabrication of semi-conductor devices[19]. Due to the high electron mobility, graphene transmits 97.1% of incident white light[20]. This number allows the graphene to be seen under an optical microscope on a SiO_2 substrate on Si. This is remarkable considering it is only one atom thick. By choosing the right oxide thickness, graphene flakes can be imaged. This is used to identify monolayer graphene under an optical microscope.
Graphene and DNA can bond to one another via both hydrophobic and hydrophilic interactions. Surface carbon atoms can oxidize to form -COOH, -CO and -NH groups which can form hydrogen bonds with DNA molecules[20]. The hydrophobic type of interactions are due to $\pi - \pi$ stacking between the aromatic rings in DNA and graphene[21]. This is the main reason the strong bonding occurs[22]. This property can be be both very useful and annoying. It makes nanopore biosensing experiments harder due to sticking of DNA to graphene causing clogging[4]. At the same time it creates an opportunity to assemble stable DNA origami-graphene hybrid structures by simply bringing the two into contact.

2.4 Conductance of nanopore hybrids

A nanopore is a nanometer-sized hole in an impermeable membrane. If the pore is placed in a cell filled with an ionic liquid and an electric field is applied, ions and other charged molecules will flow through the pore. Translocation of uncharged or weakly charged molecules will create a measurable drop in ionic flux. This is the essence of a nanopore as a biosensing tool. See figure 2.7 for a schematic drawing

In this section the relevant physics of nanopore experiments will be examined. We will first look at conductance of a bare pore and then we shall model the total conductance of the pore with a permeable DNA nanoplate docked on top of it. This is referred to as a hybrid pore. A distinction is made between pores with a thick membrane (typically 20nm) such as silicon-nitride (SiN) and almost infinitely thin pores such as graphene.

2.4.1 Bare pore conductance

In a 1:1 electrolyte solution with uniform concentration, the following expression for the ionic flux can be derived using the Nernst-Planck equation[23].

$$J = \frac{z_i^2 F^2}{RT}[D_+ + D_-]cE = \sigma_s E \tag{2.1}$$

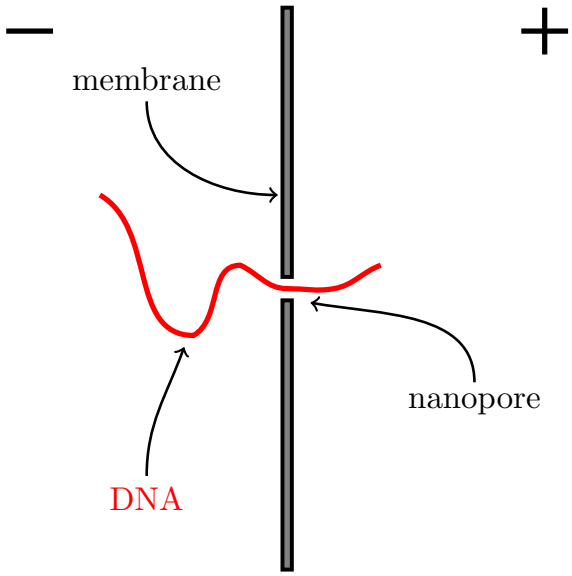

Figure 2.7: Schematic drawing of a DNA strand translocating through a nanopore

Here z_i is the charge of ion i , F is Faraday's constant, R is the ideal gas constant, T is the temperature, $D_{\pm}$ is the diffusion coefficient of the anion and cation respectively, c is the electrolyte concentration, σ_s is the solution conductivity and E is the electric field. It is assumed that the pore resistance is much larger than the resistance of the solution and than the resistance at the electrode-solution interface, this is especially the case if the solution has high conductivity[23]. The potential drop over the pore is then roughly equal to the applied bias voltage. If the pore length is much larger than its diameter $L \gg d$ the electric field inside the pore is uniform and can be approximated by $E \approx V_{bias}/L$, where L is the pore length. In figure 2.8 a schematic of the electric field inside both a thick membrane or thin membrane pore is shown. The approximation for the electric field can be implemented in equation 2.1 and assuming cylindrical geometry, an expression for the pore current can be derived.

$$I = JA = \frac{A}{L}\sigma_s V_{bias} = \frac{\pi d^2}{4L}\sigma_s V_{bias} \tag{2.2}$$

Here A is the open pore area. Differentiating I with respect to V then yields the pore channel conductance.

$$G_{channel} = \frac{dI}{dV} = \frac{1}{R} = \frac{\pi d^2}{4L}\sigma_s \tag{2.3}$$

If the condition $L \gg d$ is no longer valid, the curved field at the pore opening determine the resistance. This is modelled using the Hall access resistance[24].

$$R_{Hall} = \frac{1}{\sigma_s d} \tag{2.4}$$

The pore channel and Hall resistance can be seen as two resistors in series[23]. Using this, an expression for the total pore resistance can be obtained.

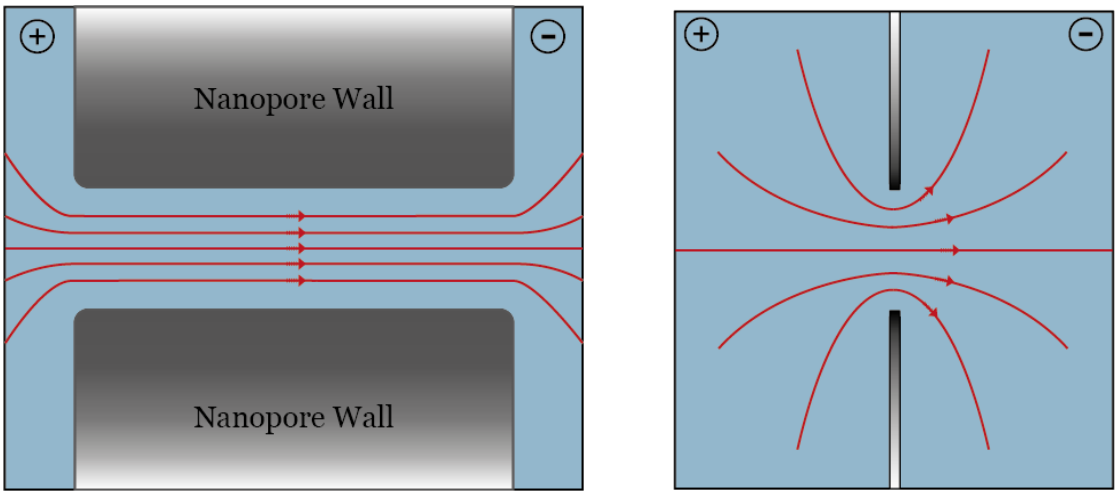

Figure 2.8: Cross section of a thick membrane nanopore (left) and a graphene nanopore (right). Red arrows represent electrical field lines.

$$R_{pore} = \frac{1}{\sigma_s}\left(\frac{4L}{\pi d^2} + \frac{1}{d}\right) \tag{2.5}$$

In the case of an almost infinitely thin two-dimensional membrane such as graphene, the pore channel contribution can be neglected and the pore conductance is simply

$$G_{pore} = \sigma_s d \tag{2.6}$$

2.4.2 Relative conductance

Our group previously investigated the ionic permeability and mechanical properties of origami-nanopore hybrid structures[5]. A similar theory shall be used here, but modified for thin graphene pores rather than SiN. The conductance of the hybrid structure can be modelled as follows[25].

$$G_{hybrid} = \left(\frac{1}{G_{plate}} + \frac{1}{G_{pore}}\right)^{-1} \tag{2.7}$$

Here the pore conductance G_{pore} is given by equation 2.6 and the plate conductance G_{plate} can be modelled by[5]

$$G_{plate} = \frac{\sigma_s \pi \alpha d^2}{4} \tag{2.8}$$

where d is the pore diameter and α is a parameter depending on the thickness and permeability of the plate.

$$\alpha = \frac{f(U)}{I_{plate}} \tag{2.9}$$

In this equation I_{plate} represents the plate thickness and $f(U)$ is a function of the fill factor and the applied potential difference. If the voltage dependence is ignored then f is simply given by $f = 1 - F$ with F the filling factor. Filling in equation 2.8 and 2.6 into 2.7 yields the following.

$$G_{hybrid} = \sigma_s \left(\frac{4}{\pi \alpha d^2} + \frac{1}{d} \right)^{-1} \tag{2.10}$$

The relative conductance is defined as the ratio of the hybrid conductance and bare pore conductance.

$$RC = \frac{G_{hybrid}}{G_{pore}} = \frac{1}{1 + \frac{4}{\pi \alpha d}} \tag{2.11}$$

This expression can be modified to display the relative conductance change.

$$\frac{\Delta G}{G} = 1 - RC = \frac{4}{\pi \alpha d + 4} \tag{2.12}$$

We can rewrite this to express the plate permeability α

$$\alpha = \frac{4}{\pi d} \left(\frac{1}{\Delta G / G} + 1 \right) \tag{2.13}$$

For a membrane which has thickness L and diameter d the relative conductance is expressed as follows.

$$RC = \frac{1}{1 + \frac{4}{\alpha(4L + \pi d)}} \tag{2.14}$$

2.4.3 Noise in graphene nanopores

For nanopores to function well as a biosensing tool it is critical that they have high signal-to-noise ratio. The signal to noise ratio is defined as the ratio between the change in current divided by the root-mean-square value I_{rms} of the baseline current.

$$I_{rms} = \sqrt{\frac{1}{N} \sum_{i}^{N} (I_i - \langle I \rangle)^2} \tag{2.15}$$

$$SNR = \frac{\Delta I}{I_{rms}} \tag{2.16}$$

Noise in nanopores is characterized by two regimes, low frequency noise ($f < 100$Hz) and high frequency noise ($f > 1$kHz)[26]. The high frequency noise power is dominated by the membrane capacitance, while the low frequency noise is characterized by a $1/f$ dependency[27]. It is theorized that $1/f$ noise is related to fluctuations

in the number and/or mobility of charge carriers[28]. Hooge's model would predict that the $1/f$ noise is inversely proportionate to the effective pore volume and consequently with the pore diameter and channel length[29,27]. This prediction proved to be accurate in SiN pores[26]. Our group previously investigated $1/f$ noise in graphene nanopores[27] and it was shown that the noise power does not depend on pore diameter, salt concentration or pH. It was found however that using thicker graphene membranes reduced noise significantly. It was proposed that the noise is caused mainly by mechanical membrane fluctuations. These fluctuations are reduced by increasing the membrane stiffness by using thicker flakes or possibly by reducing the area of free standing graphene.

Chapter 3

Methods

In this section, the experimental methods for fabricating graphene nanopores, honeycomb plate docking and analysis shall be discussed. The goal of the experiments is to find trends and characteristics of the changes in conductivity and noise in DNA-nanopore hybrids with respect to bare graphene pores and compare the results, where possible, to SiN. It shall also be determined whether the plates stick to the pore when EDTA is added to the buffer.

3.1 Nanopore fabrication

Graphene nanopores are fabricated by placing a graphene flake over a thin membrane with a small hole. The size of this hole ranges from 60nm to 1 μm. The next step is to make nanometer sized pore in the graphene using a transmission electron microscope or *TEM* for short. The process of preparing graphene flakes and placing them on a target is called *wedging transfer*[30]. The wedging transfer and TEM drilling shall now be discussed.

3.1.1 Wedging transfer

In 2010 a simple way to transfer nanostructures from one substrate to another was developed by our group[30]. The method is based on hydrophobic interactions between the material to be transferred and the target substrate. First graphene flakes are created through mechanical exfoliation of natural graphite onto a plasma cleaned Si-wafer with a 90nm thick SiO_2 substrate. These flakes can be viewed under a normal optical microscope. Flakes of different thicknesses can now be observed. Amongst them, flakes of few and monolayer graphene are present. In figure 3.1 a thick carbon flake with monolayer graphene attached to it is displayed. The flakes have dimensions in the order of microns. The next step is to submerge the silicon chip in a solution of a hydrophobic polymer cellulose acetate butyrate (CAB) in ethyl acetate ($\sim$ 30 mg/ml). This process typically takes a few seconds. After drying, a thin polymer film is on top of the silicon oxide. Because of hydrophobic interactions, the graphene will stick to the CAB film. The desired graphene flake

can now be isolated by removing the appropriate parts of the film such that a small patch containing said flake remains. This removal is done by wiping the film away with a cotton tip drenched in ethyl acetate, dissolving the polymer. The chip with the patch of film is now held under water at a given angle. Because both CAB and silicon are hydrophobic, a thin layer of water forms between the chip and the film, causing the latter to slide off and float on top of the water. Then it can be placed on the target substrate and positioned accurately by means of a needle steered by piezo mechanics, see fig 3.2. The film is then left to dry so that it sticks to the surface. When the drying is complete the chip is submerged in ethyl acetate to dissolve the film. The graphene flakes, previously embedded in the polymer film, will now stick to the surface of the target substrate due to van der Waals-interactions.

3.1.2 TEM drilling

The chips on which the graphene flakes are transferred are made of Si with a 200nm SiN substrate on top. On top of the substrate a 200nm thick platinum heating coil is deposited. Using KOH etching, a 600×600 μm free standing membrane of SiN is created. This membrane is referred to as 'the window' (see figure 3.2). Holes are drilled in the windows using a focused gallium beam (300pA) (FEI DualBeam Strata 235). Over these holes, the graphene flakes are placed using the wedging transfer described in the previous paragraph. The size of the holes determines the free-standing area of the graphene. After the graphene has been transferred onto the target, the pores can be drilled. The microscope used is a FEI titan 80-300 in STEM mode. The chip is placed in a vacuum chamber and the window is heated to $\sim 600^\circ$ Celsius. Electrons are accelerated by a potential difference of 300kV, knocking carbon atoms out of the lattice and creating a pore. The beam diameter is 0.1nm and the electron current is 0.15nA. A high temperature ($> 500^\circ$ Celsius) is then used to recrystallize the carbon surrounding the pore as the electron beam causes amorphization to some degree. Figure 3.3 displays a STEM image of a 15nm graphene pore.

Figure 3.1: Graphene flakes on a Si/SiO2 wafer

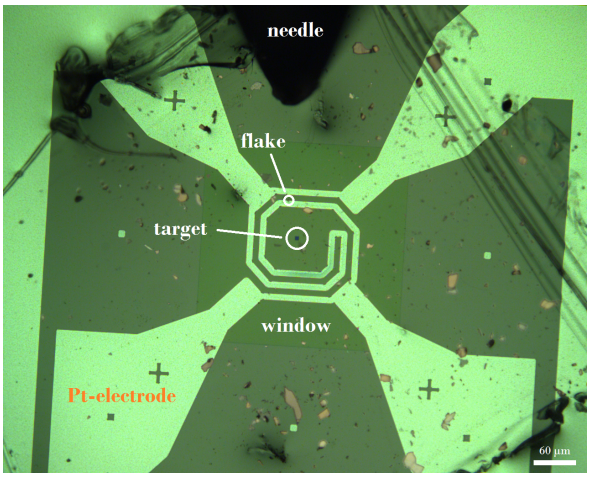

Figure 3.2: Graphene flakes embedded in a CAB patch, steered by a piezo needle

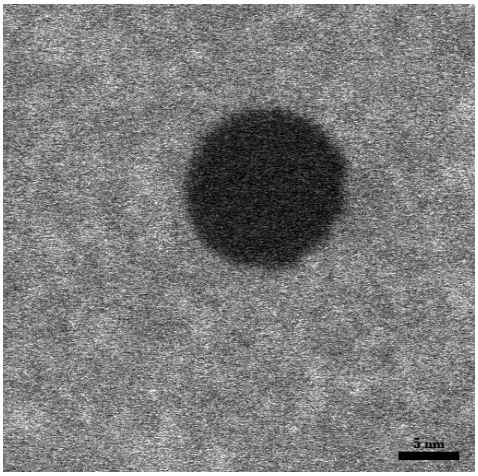

Figure 3.3: STEM image of a graphene nanopore

3.2 Nanoplate docking

The chip containing the nanopore is clamped in between a dual chamber polyether ether ketone (PEEK) flowcell filled with a buffer solution containing KCl and 'Tris' tris(hydroxymethyl)aminomethane) $(HCOH_2)_3CNH_2$, see figure 3.4a. The concentration of Tris is kept at a constant 10mM and the salt concentration is varied from 0.3M to 0.6M to 1M. Ag/AgCl-electrodes are used to create an ionic current in the flowcell and through the pore. This current is measured, filtered, amplified by an Axoclamp 200B amplifier and sent to a measurement computer by the axoclamp. *Clampex* is used to live display the current and *Clampfit* is used to analyze the data. First the baseline current at 0mV and 100mV is measured and an I-V curve is taken where the voltage is varied from -800mV to 800mV and the current is measured. A symmetrical nanopore should have a symmetrical I-V curve. As can be seen from equation 2.6, the bare pore conductance G_{bare} does not depend on the applied bias voltage. This means the pore resistance should obey Ohm's law and the I-V curve is expected to be linear. A solution of 200pM of DNA honeycomb plates is flushed into the flowcell. The plates in this work are prepared in the same way as in the SiN study[5]. The honeycomb plate contains 7560 base pairs. Its lateral dimensions are 45nm by 52nm and it is 6.75 nm thick. Due to their negative charge, the plates will move towards the positive electrode, in the opposite direction of the current. The goal is to get the plates to dock on the pore. To aid the docking process, the plates are equipped with a loop tail functioning as an anchor. See fig 3.4b for a schematic drawing. The length of this tail varies from 648 to 749 bp. The plate is permeable to ions and will thus not completely close the pore. The ratio of the conductance before and after docking is labelled the relative conductance $RC = G_{after}/G_{before}$, the absolute difference between conductance before and after docking is labelled the absolute conductance change ΔG. The ratio between the absolute conductance and the conductance pre-docking is labelled the relative conductance change $\Delta G/G$. The noise characteristics of hybrid and bare pores are determined by taking the value I_{rms} and dividing it by the mean value of the current I. See figures 3.4c and 3.4d for an illustrative drawing.

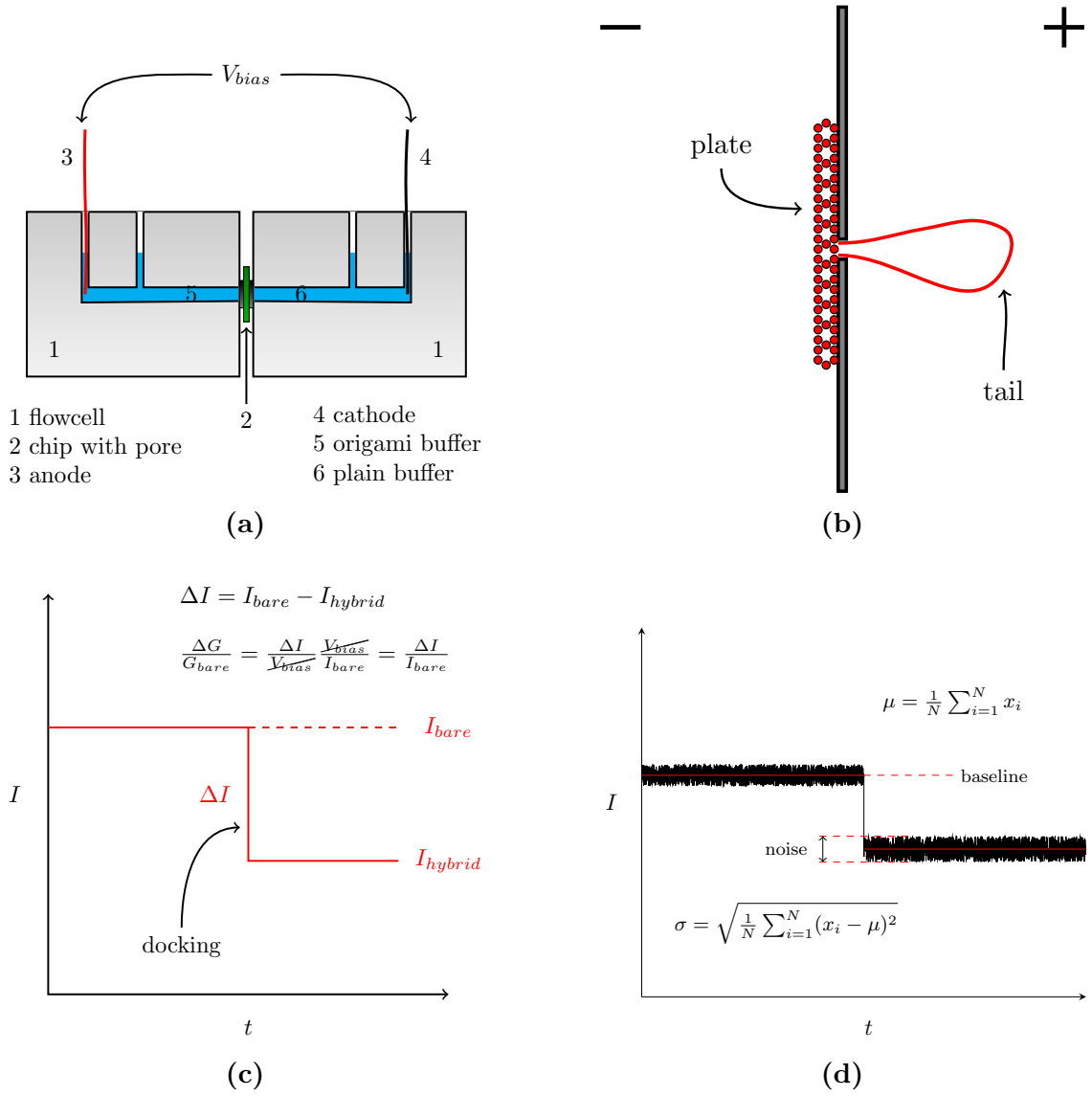

Figure 3.4: (*a*) Schematic drawing of the measurement setup, (*b*) illustrative drawing of a honeycomb plate docked onto a graphene nanopore, (*c*) illustrative scheme of the protocol for determining the relative conductance, (*d*) illustrative scheme of the protocol for determining noise characteristics of hybrid and bare pores

3.3 Sticking of plates to the pore

Graphene is subject to hydrophobic interactions with DNA. It is therefore possible that DNA sticks to a graphene membrane or even clogs the pore[4]. During preliminary experiments, the suspicion arose that in the presence of EDTA this sticking effect was even more pronounced. To test this hypothesis, a plate will be docked into the pore and subjected to a ramping negative voltage. The voltage will start at 0 and then decline to -800mV. The voltage at which the plate is ejected from the pore is a measure for the binding strength. These voltages shall be measured with 10mM EDTA and without EDTA and it shall be determined whether the plates are more likely to stick to graphene when EDTA is present or not.

Chapter 4

Results and Discussion

In this section the results of the experiments described in the methods section are presented and discussed. In section 4.1 we dock honeycomb DNA nanoplates in solutions of 0.3M, 0.6M and 1.0M KCl and vary the voltage between 100mV, 200mV and 300mV. The ratio of the conductance before and after docking is labelled the relative conductance (abbreviated as RC), the absolute difference between the conductance before and after docking is labelled the absolute conductance drop and the ratio between the absolute conductance drop and the conductance before docking is labelled the relative conductance drop. In section 4.2 we dock a plate onto a pore and subject it to a negative ramping voltage and measure the current. We repeat this measurement after adding 10mM EDTA to the buffer. In this experiment we try to confirm whether the plates stick to the pore and if sticking is more likely to occur in the presence of EDTA. In section 4.3 we compare the noise levels of hybrid pores to bare pore, where we vary the salt concentration and voltage in the same way as in section 4.1. All graphene pores used had a TEM diameter of 15nm.

4.1 Characterization of the relative conductance

Bell et al. found that DNA origami structures are in fact very permeable to ions[31]. This leads to a finite conductance after docking of a plate on the pore. Here we characterize the relative conductance as a function of voltage and salt concentration and compare the results to SiN[5].

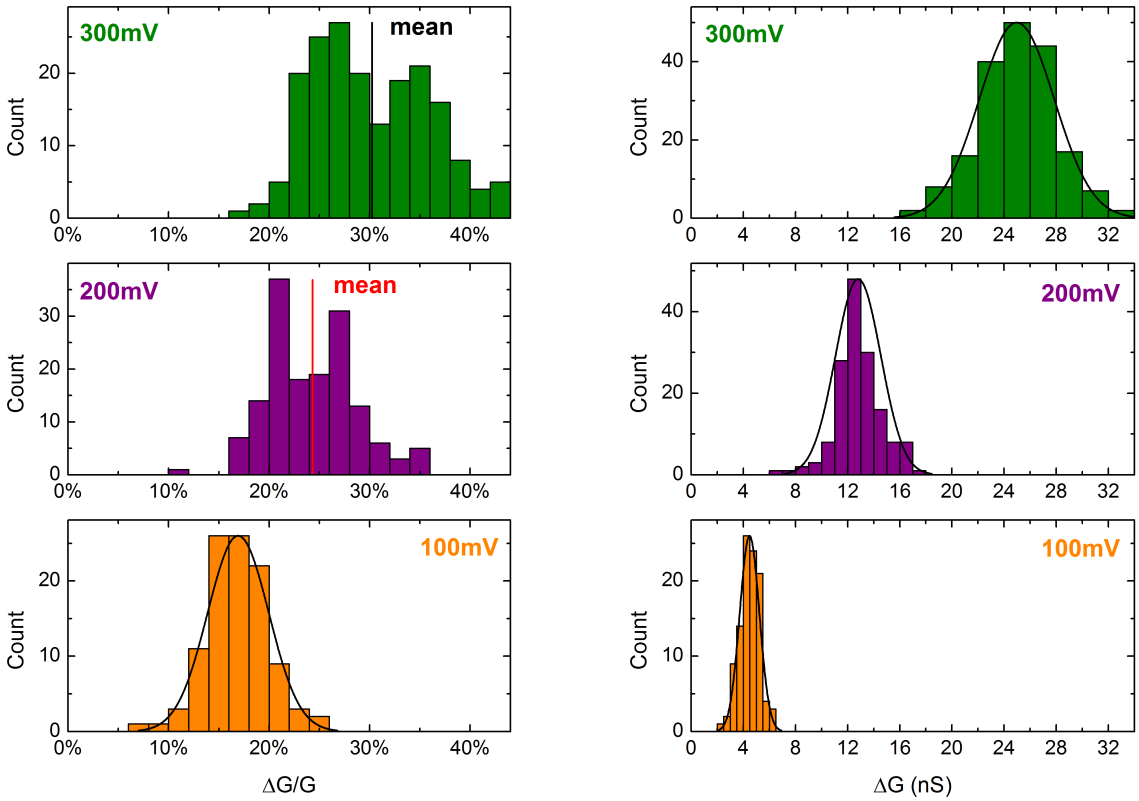

Figure 4.1: Distribution of the relative conductance drop (left) and absolute conductance drop (right) in 1.0M KCl for bias voltage 100mV, 200mV and 300mV. The figure shows data from 446 docking events. The relative conductance drop increases with voltage. For the relative conductance drop, the distribution appears to be bi-normal at 200mV and 300mV. The absolute conductance drop also increases with voltage but does not display bi-normal distributions, in contrast to the relative conductance drop.

In figure 4.1 the distributions of the relative and absolute conductance drop in 1.0M KCl for various voltages are shown. It was observed that both the relative and absolute conductance drop increased as a function of voltage. This is what was expected, as this was also found in the SiN study[5]. It was also expected that both the relative and absolute conductance drop would be normally distributed. However, the relative conductance drop shows a bi-normal distribution at 200mV and 300mV, where the absolute conductance drop shows a normal distribution. In the SiN study[5] it was found that the plates have different mechanical modes, corresponding to different conductances. This could explain the multiple peaks observed in the relative conductance drop, but fails to explain the absence of multiple peaks in the absolute conductance drop distribution. If we look at equation 2.12

$$\frac{\Delta G}{G} = 1 - RC = \frac{4}{\pi\alpha d + 4}$$

we see that an increase in pore diameter during the measurement can also cause a change in relative conductance drop, but again fails to explain the absence of a multi-variate distribution in the absolute conductance drop. Because an increase in G leads to an increase in ΔG and thus the ratio $\Delta G/G$ remains unchanged.

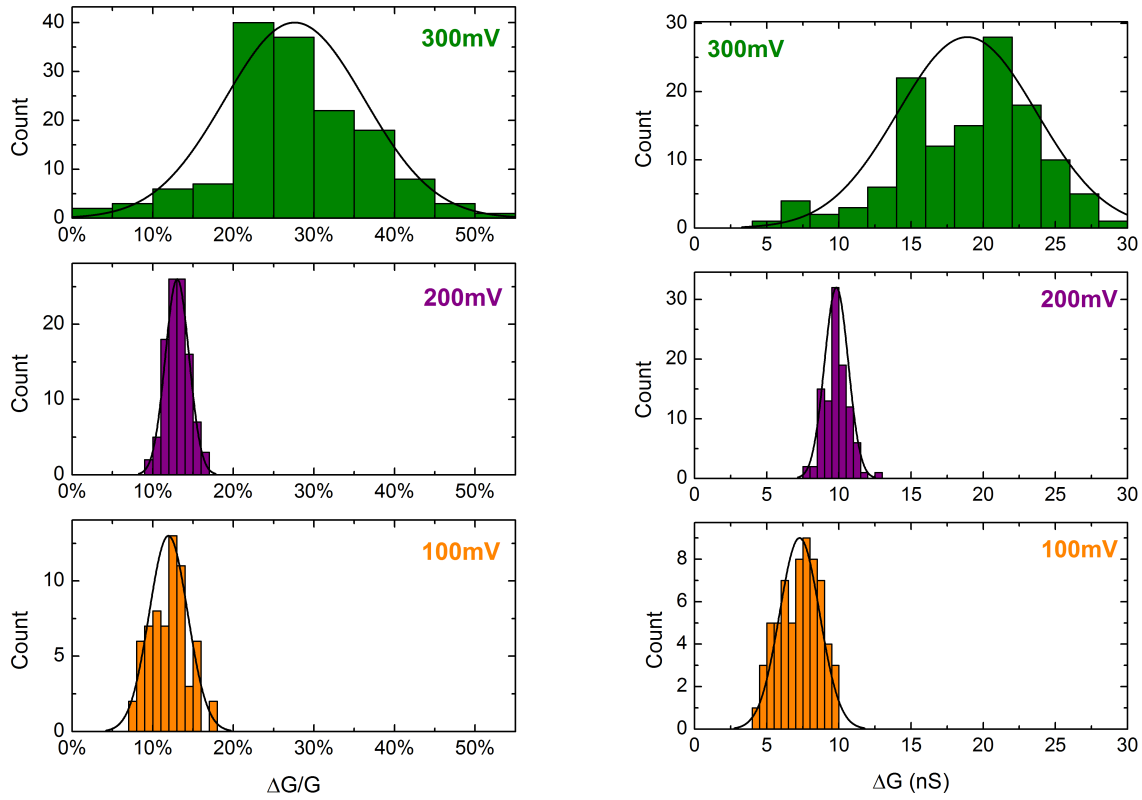

Figure 4.2: Distribution of the relative conductance drop (left) and absolute conductance drop (right) in 0.6M KCl for bias voltage 100mV, 200mV and 300mV. The figure shows data from 327 docking events. The relative conductance drop does not increase significantly as the voltage is increased from 100mV to 200mV, whereas the change from 200mV to 300mV is significant. At 300mV, the width of the distribution is much wider than at lower voltages. The absolute conductance shows a steady increase from 100mV to 200mV and from 200mV to 300mV. Again at 300mV, the distribution width is large.

In figure 4.2 the distributions of the relative and absolute conductance drop in 0.6M KCl for various voltages are shown. Here, we also observe an increase in relative and absolute conductance drop with voltage, with the exception of the data for the relative conductance drop at 200mV, where the increase from 100mV to 200mV is small. The measurement in 0.6M at 200mV was done twice, yielding similar relative conductance in both cases. We attribute the this outlying data point to non-representative measurement conditions. A possible cause could be a faulty or clogged pore.
Another interesting observation is the large width of the distributions at 300mV compared to the measurements at 100mV and 200mV. This could be due to a faulty pore or possibly a bad batch of plates, where some plates could be damaged and thus have different conductance properties.

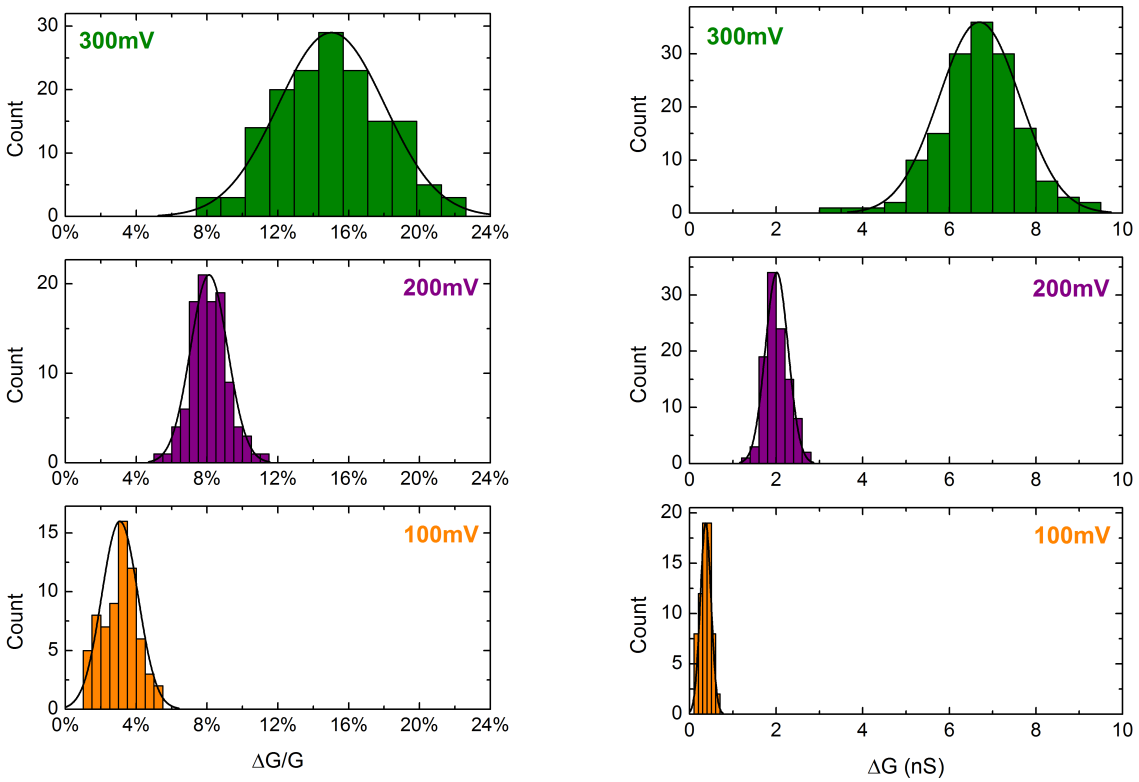

Figure 4.3: Distribution of the relative conductance drop (left) and absolute conductance drop (right) in 0.3M KCl for bias voltage 100mV, 200mV and 300mV. The figure shows data from 315 docking events. relative conductance drop increases with voltage in an almost linear fashion. At 100mV the plates hardly cause a drop in conductance. The absolute conductance also increases with voltage but not in a linear fashion.

In figure 4.3 the distributions of the relative and absolute conductance drop in 0.3M KCl for various voltages are shown. Again an increase of the relative and absolute conductance drop is observed as was expected. All distributions are normal and show an increased width as the voltage increases. At 100mV both the relative and absolute conductance drop are very small. This indicates that the plates are very leaky. In the SiN study[5] it was also found that at low ionic strength and voltage, the plates exhibited high permeability. This was concluded to be due to increased electrostatic repulsion between neighbouring strands of the origami plate.
Figures 4.1 through 4.3 all display an increased distribution width at 300mV, with respect to 100mV and 200mV. This might be explained by increased mechanical fluctuations of the plate on the pore, due to the larger forces on the plate because of the higher voltage.

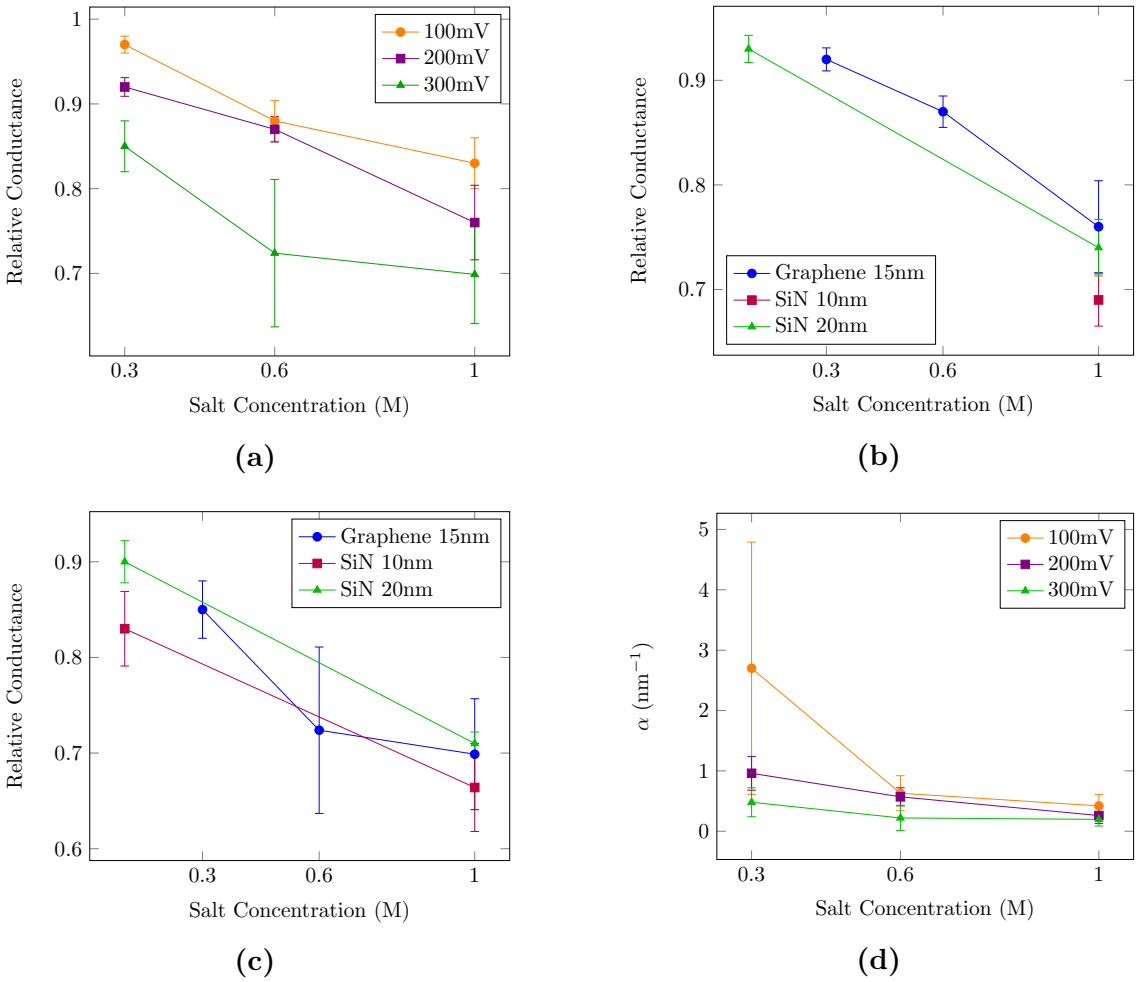

Figure 4.4: (*a*) The relative conductance of graphene-origami hybrids is displayed as a function of salt for various voltages. The figure shows data from 1088 docking events. The relative conductance appears to be a decaying function of salt concentration, with the exception of the data point at 0.6M for the 200mV line. (*b*) The relative conductance for graphene and SiN displayed as a function of salt for different pores at bias voltage 200mV. Graphene shows a higher relative conductance than SiN at any given salt. (*c*) The relative conductance is shown for graphene and SiN as a function of salt for different pores at bias voltage 300mV. Here, graphene appears to have a similar relative conductance as SiN. (*d*) The plate permeability α plotted as a function of salt concentration for graphene. The permeability decreases with salt concentration and voltage. The lowest permeability recorded is 0.197 ± 0.111 nm^{-1} for graphene, which is about twice as high as was found in SiN[5], under the same measurement conditions. Error bars indicate the standard deviation. SiN data used with permission[5]. Error bars denote the standard deviation.

In figure 4.4a the results from figures 4.1 through 4.3 have been summarized in a relative conductance ($RC = 1 - \Delta G/G$) versus salt concentration plot, for different voltages. It is observed that the relative conductance is a decaying function of salt concentration and voltage. The lowest relative conductance measured was 0.6988 ± 0.058, at 300mV in 1.0M KCl. This value is roughly the same as the relative conductance found in SiN[5], under the same measurement conditions. The data point for $V_{bias} = 200$mV at 0.6M is odd, we did not expect it to be so close to the 100mV data. As discussed earlier, we attribute this to a non-representative measurement.

Figure 4.4b compares the relative conductance of graphene and SiN at 200mV as a function of salt concentration. We see that the relative conductance of graphene is slightly higher than SiN at any given salt. In figure 4.4c the voltage is increased to 300mV and it is observed that the relative conductances of graphene and SiN are now roughly equal.

In figure 4.4d the plate permeability α is calculated from the relative conductances in figure 4.4a by means of equation 2.13, which reads

$$\alpha = \frac{f(V_{bias})}{I_{plate}} = \frac{4}{\pi d}\left(\frac{1}{\Delta G/G + 1}\right)$$

We observe that α decreases with salt concentration and voltage. This decaying trend of α with voltage can be explained by electric forces compressing the plate, which make it less permeable to ions. The highest value of α was 2.7 ± 2.1 nm^{-1}, measured at 100mV in 0.3M KCl. At this voltage and salt concentration, the plates exhibit very high permeability. The lowest value of α was found to be 0.197 ± 0.111 nm^{-1}, measured at 300mV in 1.0M KCl. This value is roughly twice as high as the values found in the SiN study[5]. This is remarkable, as one would expect α to be an intrinsic property of the plate itself, rather than the type of pore it is positioned on. To explain the discrepancy, the model (equation 2.13) should be reassessed. The hydrophobic interactions between the graphene and origami plates can perhaps play a role.

4.2 Sticking of plates to graphene nanopores

In preliminary experiments, it was observed that when plates were docked onto a pore, they were very hard to undock when EDTA was in the buffer solution. This lead to the hypothesis that with EDTA, DNA plates are more likely to stick to the graphene pore. In this section, we test this hypothesis by docking a plate and subjecting it to a negative ramping voltage and measuring the current.

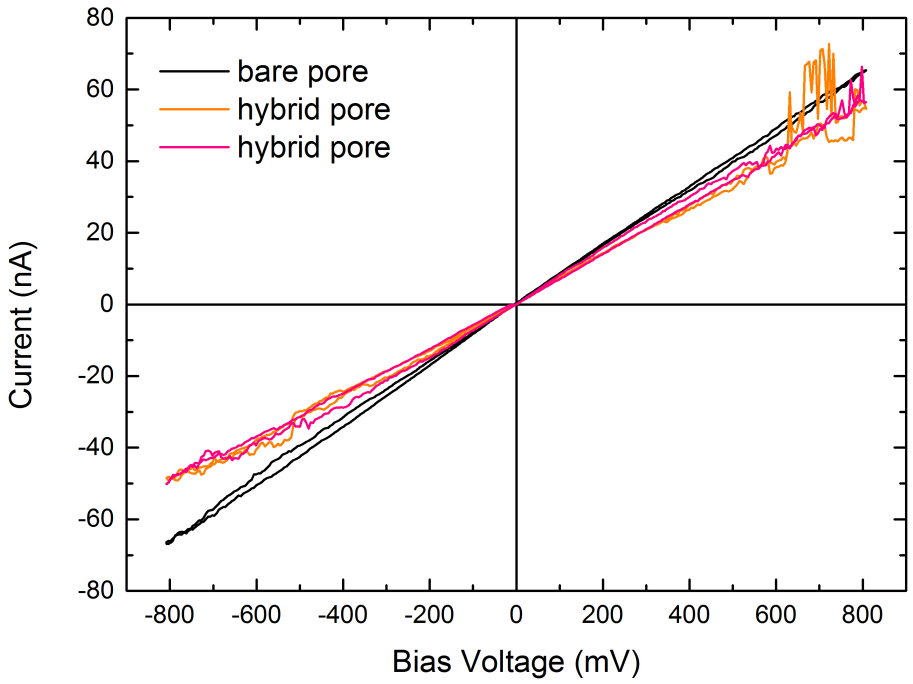

Figure 4.5: Comparison between I-V curves of a bare pore (black) and 2 hybrid pores (coloured) in 1.0M KCl (no EDTA). The voltage is ramped up to 800mV, then ramped down to -800mV and then back up to 0mV. The I-V curve of the bare pore curve is linear and thus obeys Ohm's law. The hybrid pores show lower conductance than the bare pore. At around 600mV, the orange line shows strong fluctuations. This can also be seen in the magenta line, though not as pronounced. In the negative regime, a clear difference in conductance properties between both hybrid pores and the bare pore can be seen. The hybrid conductances are lower and exhibit non-linear behaviour.

Figure 4.5 shows I-V curves of a bare pore and 2 hybrid pores. From the I-V curves, it is easy to distinguish when there is a plate on the pore and when there is not. The curves of hybrid pores show lower conductance, even in the negative regime. This suggests that the plate might stick to the pore. We docked plates and subjected them to the negative regime of the I-V curve shown in figure 4.5, e.g. we ramp the voltage from 0mV down to -800mV. This was done for 2 different buffers, one plain buffer (1.0M KCl 10mM Tris) and one with 10mM EDTA.

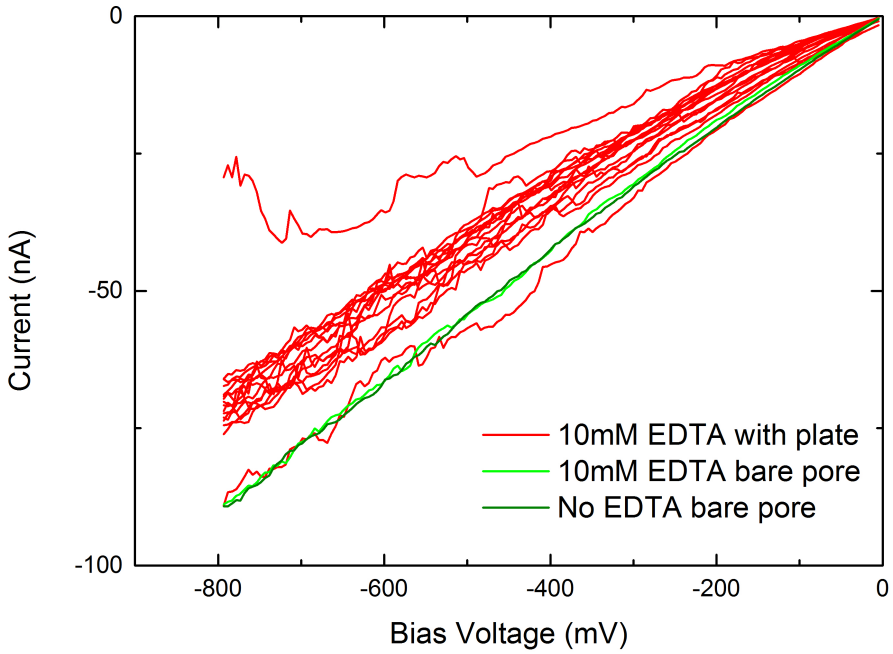

Figure 4.6: All negative I-V traces of bare pores (green) and pores with a plate docked at the start (red) in 1.0M KCl with 10mM EDTA. The graph displays 18 traces, of which 2 represent bare pores and 16 represent traces with plates on top. The average conductance of all red lines was found to be 88.2nS. No significant difference between bare pore traces with and without EDTA is observed (114.5 vs. 114.9nS respectively). Of the red traces, 15 out of 16 show significantly lower conductance (on average $\sim 30\%$ lower) than the bare pore. One red trace is in agreement with the bare pore. Traces with EDTA show more fluctuations than the bare pore, especially at high negative voltages.

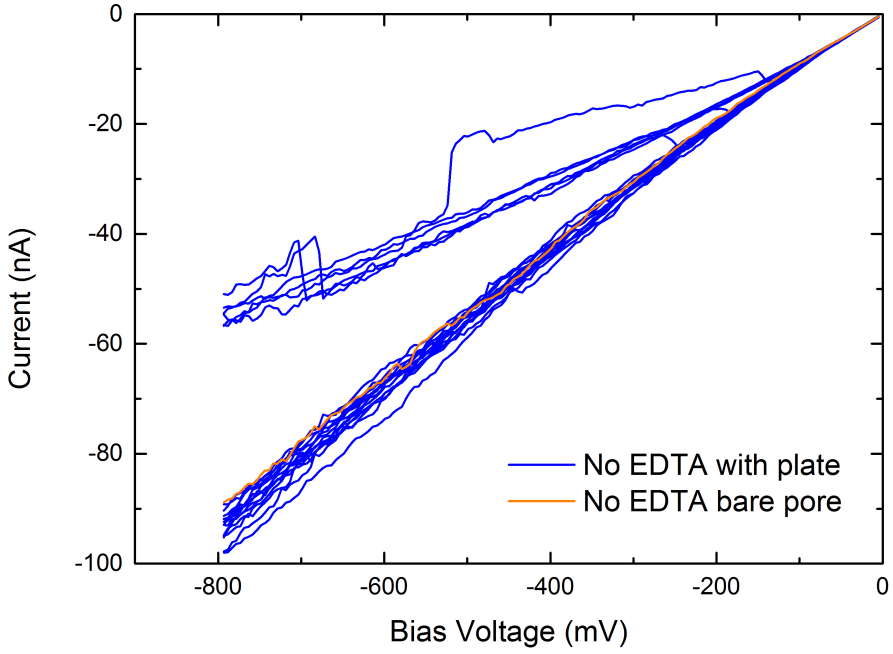

Figure 4.7: All negative I-V traces without EDTA. The figure shows 19 lines of which one represents the bare pore (orange) and 18 represent hybrid pores. Of all 18 hybrid pore curves, 14 are in agreement with the bare pore curve. The remaining 4 show 42% lower conductance than the bare pore and also show stronger fluctuations.

In figure 4.6, all negative I-V traces with 10mM EDTA are shown. It is observed that there is no significant difference between bare pore I-V curves with and without EDTA. Most traces have about 30% lower conductance than the bare pore. This could be interpreted in a number of ways. It is possible that the hypothesis is true and the plates stick to the pore, or the plate that was on top initially diffuses out at the start and another plate is captured from the other side. If the latter happens, it would most likely be at the start of the trace, since no clear sudden conductance drops, with respect to the bare pore, were observed.
Figure 4.7 shows all traces without EDTA. We observe that most traces are in agreement with the bare pore I-V. This suggests that sticking is not as likely without EDTA, as it is with. There is also a number of traces that show significantly lower conductance than the bare pore I-V. Some of these traces exhibit sudden jumps that could be interpreted as plate captures. These traces also exhibit a higher conductance drop than traces with EDTA (figure 4.6). Possibly, pore-plate interaction is affected by the presence of EDTA.

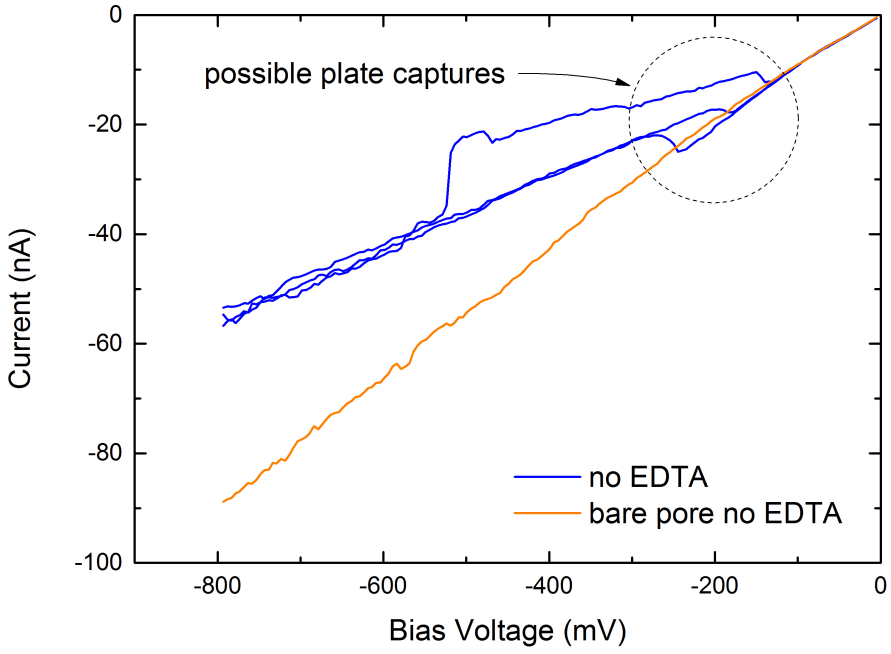

Figure 4.8: Several traces without EDTA (blue) that show strange behaviour. Traces exhibit sudden drops in conductance after following the bare pore curve (orange) initially. This is believed to be caused by plate captures, after the plate that was on top initially, has diffused out. Measurements were conducted in 1.0M KCl.

Figure 4.8 shows a number of traces selected from figure 4.7 that show sudden drops in conductance. The traces follow the bare pore curve initially, and then suddenly the conductance drops. This observation corresponds to the capture of a plate as was demonstrated in previous work[5]. As mentioned earlier, this could mean that the plate that was on top initially diffused out and another plate from the opposite side is captured. It is also possible that 2 plates were docked simultaneously, this would explain the remarkably low conductance. The traces with EDTA from figure 4.6 do not show these sudden jumps. It is therefore assumed that in said traces, no plate captures occur.

4.3 Noise of hybrid and bare pores

It is proposed[27] that membrane fluctuations are a major source of noise in graphene nanopores. Theoretically, docking a plate on a graphene nanopore might stiffen the structure and reduce noise. Noise levels in SiN pores are typically lower than in graphene[27], but possibly the plates could reduce the noise in graphene to rival SiN. Here we compare the noise levels of bare pores to hybrid pores. We measure I_{rms} before and after docking and compare both values.

In figure 4.9a (see page 35), the normalized current noise is plotted against the bias voltage in 0.3M KCl. We normalize the noise current (I_{rms}) by dividing it by the mean value of the current. We observe that noise characteristics of both bare and hybrid pores improve with bias voltage. The same trend is observed in 0.6M (figure 4.9b) and 1.0M KCl (figure 4.9c), for both hybrid and bare pores. Another trend we see, is that at lower voltages, noise levels of hybrid pores decrease with salt concentration. This is evident in figure 4.9d. At higher voltage, the noise in 0.6M was lowest, yet close to 1.0M. It was proposed that the plates might stiffen the graphene membrane and reduce pore noise by reducing fluctuations[27]. The data from figure 4.3 however, suggests that the plates increase noise, in contrast to what was expected. Possibly, the contribution of the plates to the membrane stiffness is not sufficient to effectively reduce noise. Another explanation might be that mechanical fluctuations of the plates introduces noise.

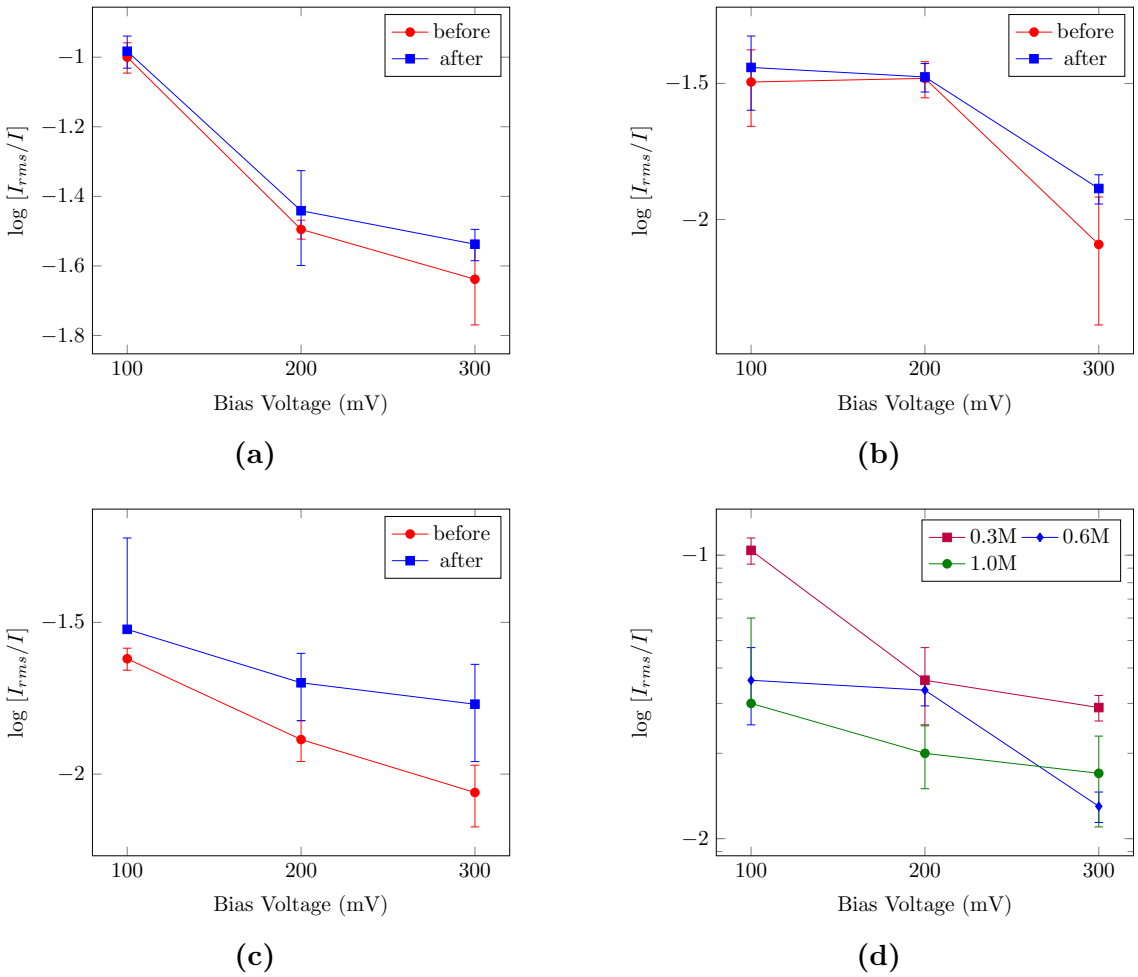

Figure 4.9: (a) The normalized noise of hybrid (blue) and bare pores (red) in 0.3M KCl is plotted against the bias voltage on a semi-log scale. It is observed that the noise characteristics improve with bias voltage. It is also observed that the difference in noise level between hybrids and bare pores increase with voltage. Hybrid pores appear to have higher noise levels than bare pores. (b) Here, the salt concentration is 0.6M KCl. A similar trend is observed as in (a), with the exception of the data at 200mV. (c) Salt concentration 1.0M KCl. Again the noise decreases with voltage. Hybrid pores have significantly more noise than bare pores at this salt concentration. (d) All data of the hybrid pores from figures (a) (red), (b) (blue) and (c) (green) summarized. It is observed that at 100mV and 200mV, the noise characteristics of hybrid pores improve with salt concentration. At 300mV, the noise was lowest in 0.6M. The figure shows data from 1088 docking events. Error bars denote the standard deviation.

Chapter 5

Conclusions

Combining DNA origami with nanopores introduces a number of advantages, such as the ability to bind proteins to a loose strand on top of a DNA origami plate for protein sensing or using a plate with an aperture to prevent DNA strands clogging the pore in translocation experiments. It is also an elegant way to create a bottom-up nanostructure with nm precision. A possible advantage of graphene over SiN in this respect, is the ability of DNA to stick to the graphene membrane. This creates a more stable hybrid and makes it possible to switch from positive to negative bias voltages during experiments. In this thesis, experiments with honeycomb DNA origami plates docked on graphene nanopores were performed. The main goals of the experiments were to characterize the relative conductance as a function of salt and applied bias voltage and to determine whether the plates stick to the pore in the presence of EDTA. The effect of the plates on pore noise was also characterized as a function of salt and bias voltage.

In section 4.1 the relative conductance as a function of bias voltage and salt was characterized. To maximize the signal-to-noise ratio, the permeability of the plate to ions should be minimized. This permeability was determined by measuring the ratio of the conductance of the bare pore and the origami-graphene hybrid. The lower the relative conductance, the lower the plate permeability. It was found that the relative conductance decreased with salt and voltage. The lowest relative conductance measured was $69.9 \pm 5.8\%$ at 300mV in 1.0M KCl, this yielded a value 0.197 ± 0.111 nm^{-1} for the plate permeability. In SiN pores, a similar value for the relative conductance was found[5], around 70%. The plate permeability found previously[5] for SiN was significantly lower at about 0.09 nm^{-1}, this discrepancy is most likely due to the incompleteness of the model used to calculate it, as the model does not take hydrophobic effects into account.

In section 4.2 it was tested whether EDTA indeed promotes sticking. Nanoplates were docked onto the pore in 1.0M KCl with and without EDTA and subjected to a ramping negative voltage. Without EDTA it was observed that 79% of traces was in close agreement with the bare pore I-V curves, in the remainder of traces it was believed that a plate from the other side was caught. This leads us to conclude that sticking is not likely to occur without EDTA. When 10mM EDTA was added to the buffer, the conductance found in most traces was roughly 30% lower than the bare pore I-V. This drop is in good agreement with the results from 4.1, which suggests

the plates stick to the pore. Of all 17 traces with EDTA, 15 showed evidence of sticking. These findings point towards the notion that the plate is more likely to stick in the presence of EDTA, but more data is needed to support this claim. A number of traces showed remarkably low conductance and strong fluctuations, it is unclear what caused this, possibly two simultaneously docked plates.

In section 4.3 the effect of the plates on pore noise has been characterized. Overall, it was found that the noise characteristics improved with salt and voltage. It was proposed that membrane fluctuations induce noise in graphene nanopores, and we studied whether the docking of plates could affect noise. It was found that the hybrid pores have slightly worse noise characteristics than bare pores. At low voltages and low salt, noise characteristics of the bare and hybrid pore were roughly equal and as the voltage increased, the hybrid pore started to perform worse.

From this study, it can be concluded that to minimize leakage of ions through DNA honeycomb plates on graphene nanopores, measurement conditions with low salt and low voltage should be avoided. It can also be concluded that EDTA might be used to fixate the plates on the pore, which can be an advantage during experiments. Lastly, plates reduce the already troublesome resolving power of graphene nanopores. In this respect, SiN is still the better option to combine DNA origami plates with solid-state nanopores, as a biosensing tool.

Chapter 6

Outlook

Origami-nanopore hybrids represent great promise as a tool for protein and DNA sensing. Whether graphene is the ideal material for this type of nanopore experiment remains to be seen. The main disadvantage of graphene in comparison to SiN is the noise characteristics. There are possible approaches however, to improve noise in graphene nanopores. If the noise is indeed caused by membrane fluctuations, reducing the area of free-standing graphene would stiffen the structure and improve noise characteristics. The pores used in the experiments in this thesis had a free standing area of 1 μm. A few graphene pores with smaller free standing areas have already been fabricated by our group and seem to have lower noise. It would be interesting to investigate what is the optimal free standing area and to see if the signal-to-noise ratio of SiN can be surpassed.
An advantage of graphene over SiN would be the sticking of the plates to the pore. The experiments done in this thesis suggest sticking, but more experiments will have to be done to confirm it indefinitely. A possible approach would be to use Atomic Force Microscopy. If sticking can be confirmed then this opens up many new possible experiments. An example is the experiment[32] our group conducted in 2013, where DNA molecules were translocated, recaptured shortly after and then re-translocated by means of a reversed bias voltage. This experiment gave much insight in the dynamics of DNA translocation through solid-state SiN nanopores. Such an experiment would be difficult to do with graphene, as the DNA usually sticks and clogs the pore. With a graphene-origami hybrid, such an experiment would be possible if the plate sticks to the pore. If it does not, the plate would just release as soon as the voltage is reversed. If the noise issue in graphene can be resolved and sticking can be confirmed, it would be an excellent candidate for use in future nanopore-DNA experiments.

Appendices

Appendix A

Data tables and buckling voltage distribution

	100mV	std	200mV	std	300mV	std
0.3M	0.97	0.01	0.92	0.01	0.85	0.03
0.6M	0.88	0.02	0.87	0.01	0.72	0.09
1.0M	0.83	0.03	0.76	0.04	0.70	0.06

Table A.1: Relative conductance

	100mV	std	200mV	std	300mV	std
0.3M	2.68	2.09	0.96	0.28	0.48	0.24
0.6M	0.63	0.29	0.57	0.15	0.22	0.21
1.0M	0.42	0.19	0.26	0.13	0.20	0.11

Table A.2: Plate permeability in units nm^{-1}

	100mV	std	200mV	std	300mV	std
0.3M	0.100	0.0103	0.0546	0.002	0.029	0.006
0.6M	0.032	0.010	0.033	0.005	0.008	0.004
1.0M	0.024	0.002	0.013	0.002	0.009	0.002

Table A.3: Normalized noise values before docking

	100mV	std	200mV	std	300mV	std
0.3M	0.104	0.011	0.059	0.002	0.033	0.008
0.6M	0.036	0.011	0.034	0.004	0.013	0.016
1.0M	0.029	0.003	0.020	0.005	0.017	0.006

Table A.4: Normalized noise values after docking

V_{bias} (mV)
-564
-350
-345
-504
-385
-370
-364
-239
-430
-420
-429
-559
-550
-340
-364

Table A.5: Voltage at which mechanical buckling was initiated, $\mu = 414.2 \pm 93.7$mV

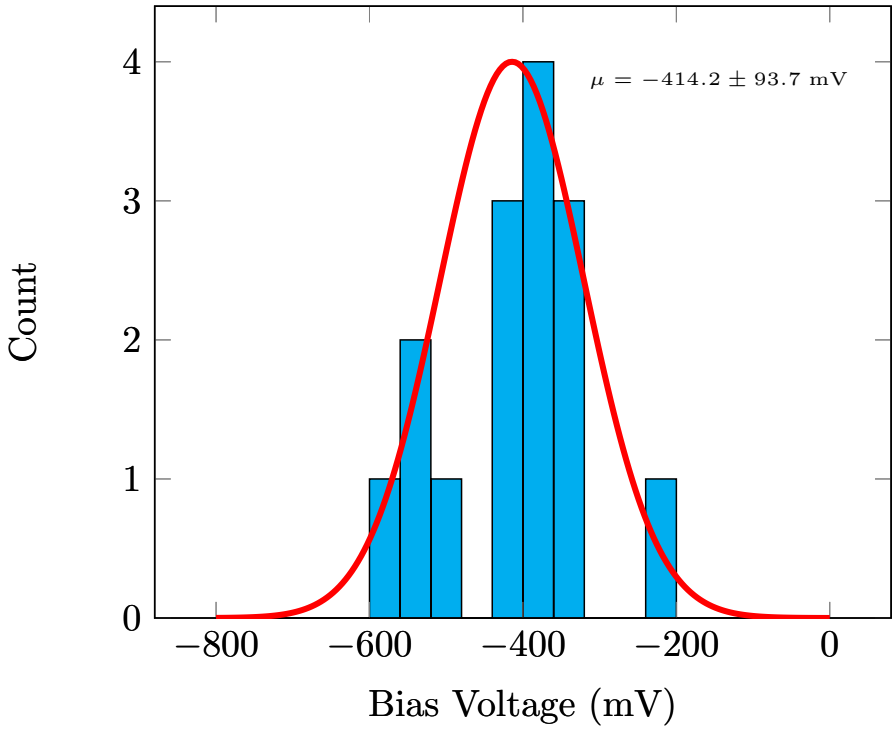

Figure A.1: Distribution of the voltage at which mechanical buckling initiated in traces with EDTA. The mean value found was -414.2 ± 93.7mV

Bibliography

[1] Kasianowicz J.J. et al. "Characterization of individual polynucleotide molecules using a membrane channel". In: *Proc. Natl. Acad. Sci. USA* 93 (1996), pp. 13770–13773.

[2] Dekker C. "Solid-state nanopores". In: *Nature nanotechnology* 2 (2007), pp. 209–215.

[3] Tang Z. et al. "Constraint of DNA on Functionalized Graphene Improves its Biostability and Specificity". In: *Small* 6 (2010), pp. 1205–1209.

[4] Schneider G.F. et al. "Tailoring the hydrophobicity of graphene for its use as nanopores for DNA translocation". In: *Nature Communications* 4 (2013), pp. 1–7.

[5] Plesa C. et al. "Ionic Permeability and Mechanical Properties of DNA Origami Nanoplates on Solid-State Nanopores". In: *ACS Nano* 8 (2013), pp. 35–43.

[6] Crick F. Watson J. "Molecular structure of nucleic acids". In: *Nature* 171.4356 (1953), pp. 737–738.

[7] Alberts B. *Molecular biology of the cell 5th edition*. New York: Garland Science, 2008.

[8] Ghosh A. and Bansal M. "A glossary of DNA structures from A to Z". In: *Acta Cryst Sect D.* 59.4 (2003), pp. 620–626.

[9] Liu Y. and S. West. "Timeline: Happy Hollidays: 40th anniversary of the Holliday junction". In: *Nature Reviews Molecular Cell Biology* 5.11 (2004), pp. 937–944.

[10] University of Dundee Nucleic Acid Structure Research Group. *Structure, Folding and Activity of Branched Nucleic Acids*. 2014. URL: `http://www.dundee.ac.uk/biocentre/nasg/research.php`.

[11] Rothemund P. "Folding DNA into nanoscale shapes and patterns". In: *Nature* 440.7082 (2006), pp. 297–302.

[12] Douglas S. et al. "Rapid prototyping of 3D DNA-origami shapes with caDNAno". In: *Nucleic Acids Research* 37 (2009), pp. 5001–5006.

[13] Douglas S. et al. "Self-assembly of DNA into nanoscale thee-dimensional shapes". In: *Nature* 459.7245 (2009), pp. 414–418.

[14] Novoselov K.S. et al. "Electric Field effect in atomically thin carbon films". In: *Science* 306 (2004), pp. 666–669.

[15] Partoens B. and Peeters F.M. "From graphene to graphite: Electronic structure around the K point". In: *Physical Review* 74.075404 (2006).

[16] Ishigami M. et al. “Atomic structure of graphene on SiO2”. In: *Nano Letters* 7 (2007), pp. 1643–1648.

[17] Novoselov K.S. et al. “Two-dimensional atomic crystals”. In: *PNAS* 2.30 (2005), pp. 10451–10453.

[18] Falkovsky L.A. “Optical properties of graphene”. In: *Journal of Physics:Conference Series* 129.012004 (2008).

[19] Geim A.K. “Graphene: Status and Prospects”. In: *Science* 324 (2009), pp. 1530–1534.

[20] Kuilas T. et al. “Chemical functionalization of graphene and its applications”. In: *Progress in Materials Science* 57 (2012), pp. 1061–1105.

[21] Premkumar T. and Geckeler K. “Graphene–DNA hybrid materials: Assembly, applications, and prospects”. In: *Progress in Polymer Science* 37 (2012), pp. 515–529.

[22] Lena Ai Ling Tang et al. “Graphene-Based SELDI Probe with Ultrahigh Extraction and Sensitivity for DNA Oligomer”. In: *Journal of the American Chemical Society* 132 (2010), 10976–10977.

[23] Gibb T. Albrecht T. and Nuttal P. *Engineered Nanopores for Bioanalytical Applications*. Oxford: Elsevier, 2013.

[24] Hall James E. “Access Resistance of a Small Circular Pore”. In: *The Journal of General Physiology* 66 (1975), pp. 531–532.

[25] Wei R. et al. “DNA Origami Gatekeepers for Solid-state Nanopores”. In: *Angewandte Chemie* 124 (2012), pp. 4948–4951.

[26] Smeets R.M.M. et al. “Noise in solid-state nanopores”. In: *PNAS* 105 (2007), pp. 417–421.

[27] Heerema S.J. et al. “1/f noise in graphene nanopores”. In: *Nanotechnology* (2014).

[28] Balandin A.A. “Low-frequency 1/f noise in graphene devices”. In: *Nature Nanotechnology* 8 (2013), pp. 549–555.

[29] Hooge F.N. “1/f noise sources”. In: *IEEE Trans. Electron Devices* 41 (1994), pp. 1926–1935.

[30] Schneider G.F. et al. “Wedging Transfer of Nanostructures”. In: *Nanoletters* 10 (2010), pp. 1912–1916.

[31] Bell N.A.W. et al. “DNA Origami Nanopores”. In: *ACS Nano* 12 (2012), pp. 512–517.

[32] Plesa C. et al. “Non-equilibrium folding of individual DNA molecules recaptured up to 1000 times in a solid state nanopore”. In: *Nanotechnology* 24.47 (2013), p. 475101.